Ultrastructural aspects of sonogels

M.C. Barrera-Solano, N. de la Rosa-Fox and L. Esquivias

Department of Structure and Properties of Materials, University of Cádiz, Apartado 40, Puerto Real, 11510 Cádiz, Spain

The ultrastructure of silica sonogel is discussed from data obtained by wide angle X-ray scattering (WAXS) and magic angle spinning nuclear magnetic resonance (MAS-NMR). WAXS data are very useful for measuring the skeletal density at the scale of angströms since the Fourier transform of the interference function of the scattered radiation implicitly involves this parameter. This is evaluated maximizing the entropy of the system to obtain an atomic radial distribution function compatible with the experimental data and, in particular, with the solid backbone density which, in the case of silica, is 2.09 g/cm^3. The results indicate that aerogels from sonogels are formed by very uniform aggregates exhibiting two levels in a hierarchical structure of near spherical-shaped particles.

1. Introduction

Sonogels [1], which are prepared without solvent in the presence of an acid catalyst, present peculiar ultrastructural properties caused both by the absence of a solvent as well as the nature of the preparation method. Thus, unlike the gels prepared by the classic method, alkoxide and water react in the vapour phase [2] inside the numerous bubbles produced by cavitation provoking the formation of many 'microgel particles' which aggregate later. This mechanism gives rise to a highly uniform pore size distribution structure which specially conforms to the Zarzycki's model hypothesis [3,4] which shows that its structure abides by a Scott's loose model [5].

The initial purpose of preparing sonogels was to have denser starting structures that could be easily densified into solid glass [6]. However, the sintering from aerogels requires a careful treatment to eliminate the organic residues and water. They are proving very promising in composite technology, where dense precursor gels or/and a short gelation time are required and they are being successfully employed to prepare homogeneously distributed composites with low-shrinkage matrices [7], corrosion resistant coatings [8] and extremely fine and uniform dispersions with photochromic and non-linear optical properties [9].

This paper presents the results of an ultrastructural study with combines local probes (^{29}Si magic angle spinning nuclear magnetic resonance (MAS-NMR) spectroscopy and wide angle X-ray scattering (WAXS)), with textural determinations (N$_2$ adsorption) of different aerogels. Radial distribution function (RDF) analysis serves as a connection between the study of material texture and the solid phase structure through the calculation of the skeletal density.

2. Experimental

The aerogels were prepared from TEOS in the way described in ref. [6]. From now on, [Sn] is used to designate a sonogel prepared with n mol water per 1 mol TEOS. [Cn] designates the corresponding classic gel, obtained with a dilution of 3 mol EtOH/mol TEOS.

For WAXS measurements, aerogels were ground to fine powders (< 40 μm) and compacted into bricks by pressure. Intensities were measured on a D500 Siemens diffractometer equipped with conventional Bragg–Brentano geometry and DACO-MO automatic step scanning.

Both Cu and Mo K_α anodes ($\lambda = 1.542$ Å and 0.711 Å, respectively) were used in order to cover a wider interval of scattering vector modulus, $s = (4\pi/\lambda) \sin\theta$, as well as to reduce the problems of absorption correction with samples without 'infinite thickness'.

Four series of monochromatized radiation data were collected in step size $2\Delta\theta = 0.5°$, by means of a scintillation counter, in the intervals 0.45 Å^{-1} $< s <$ 6.70 Å^{-1} with Cu and 6.70 Å^{-1} $< s <$ 14.50 Å^{-1} with Mo anode. The number of counts was never less than 2000. Mean values of those measured in each observation were assigned to that position. Data were normalized into electronic units by the high angle method [10], and then the Compton scattering was substracted.

^{29}Si solid state spectra were recorded at room temperature on a Bruker MSL400 spectrometer at the frequency of 79.5 MHz. Spinning rates were between 1 and 4 kHz. The chemical shift is referenced to TMS.

Specific surfaces were obtained by Brunauer-Emmett-Teller (BET) analysis using nitrogen adsorption.

3. Skeletal density calculation from WAXS data

Backbone densities were calculated by the maximum entropy method (MEM) [11] which gives the RDF of an arrangement of atoms as the one corresponding to the atomic distribution compatible with diffraction data and density at the scale of the X-ray wavelength.

The entropy, S, of a structure with spherical symmetry composed by N scattering centres distributed over M spherical shells of radius r_j and Δr thick is

$$S = CN \ln N - C \sum_{j=1}^{j=M} 4\pi r_j^2 \, \Delta r \rho(r_j) \, \ln\rho(r_j),$$

where C is a constant and $\rho(r_j)$ is the radial density of scattering centres in the j-shell.

The experimental constraints set up a system of $(L + 1)$ equations:

$$\sum_{j=1}^{j=M} 4\pi r_j^2 \rho(r_j) = \sum_{j=1}^{j=M} 4\pi r_j^2 \rho_0$$
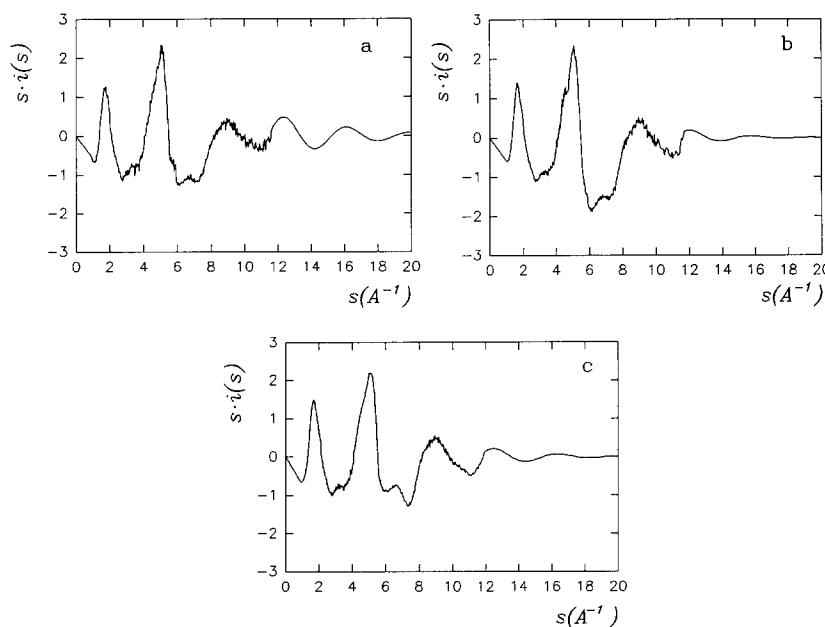
Fig. 1. Interference function theoretically extended. From 0 to s_{min} are linearly extrapolated. (a) [C4], (b) [S4], (c) v-SiO$_2$. The more discontinous structure of [C4] is evident from the increase of intensities at low s.

for the macroscopic density, besides the L equations

$$\sum_{j=1}^{j=M} \pi r_j^2 \left[\rho(r_j) - \rho_0\right] \frac{\sin(r_j s_I)}{r_j s_j} \Delta r = i(s_I),$$

$$I = 1, 2, \ldots, L,$$

which correspond to the Fourier inversion of the L values of the structure factor,

$$i(s) = \frac{I_{e.u.} - \Sigma x_i f_i^2}{(\Sigma x_i f_i)^2},$$

where x_i and f_i are, respectively, the atomic fraction and amplitude of the ith element. $I_{e.u.}$ are the intensities in electronic units after corrections. The problem may be satisfactorily solved by means of Lagrange multipliers leading to the result

$$\rho(r_j) = \exp\left[-1 - \mu_0 - \mu_I \operatorname{sinc}(r_j s_I)\right],$$

where the μ_0, μ_I, ... are the unknowns to be evaluated. In this case, the highly non-linear sys-

tem is solved numerically by means of an algorithm based on the Newton method [12], with the initial values $\mu_0 = -1 - \ln \rho_0$ and $\mu_1 = 0$, for $I = 1, 2, \ldots, L$. Thus, this procedure allows for a reliable estimate of the materials' real microscopic density to be obtained as the $\mu_0 = -1 - \ln \rho_0$ Lagrange multiplier is an adjustable parameter of the problem.

4. Results

4.1. X-ray scattering

The interference functions (fig. 1) of gels show less intense and broader maxima than v-SiO$_2$; also, their positions are shifted toward higher s values. Other features are the absence of a characteristic vitreous silica shoulder between 2.2 and 2.7 Å^{-1} [13] and a significant drastic increase in depth of the minimum located at 6 Å^{-1} in the gel pattern.
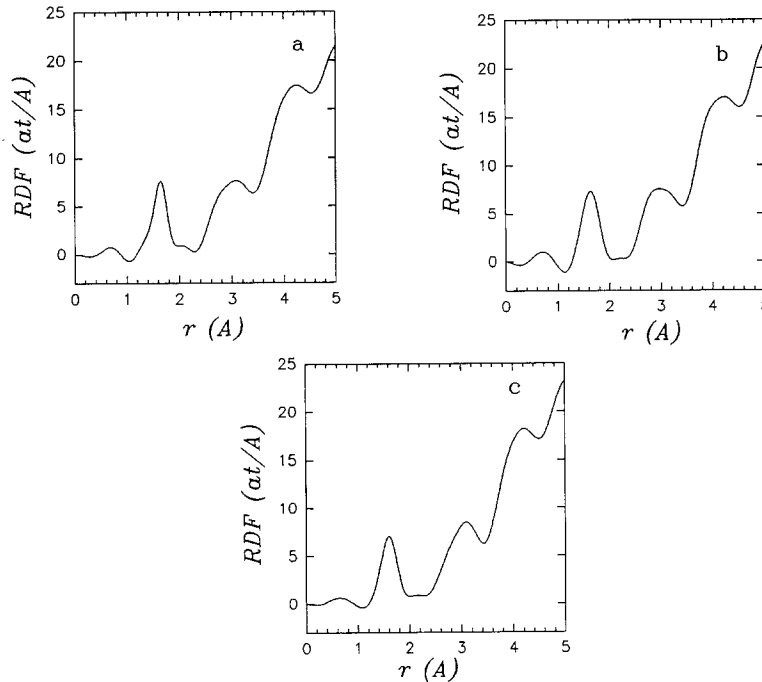
Fig. 2. RDFs from the substitution in eq. (1) of the calculated densities. Table 1 gives the main structural parameters. (a) [C4], (b) [S4], (c) v-SiO$_2$, Si–O non-bridging bonds (standard distance 1.54 Å [15]) cause a slight shift in the adjacent bridging Si–O bond distances and tetahedra network distortion as it is reflected in the flattening of the second maxima.

$$r\ G(r)\ (at/A)\quad v.s.\quad r\ (A)$$
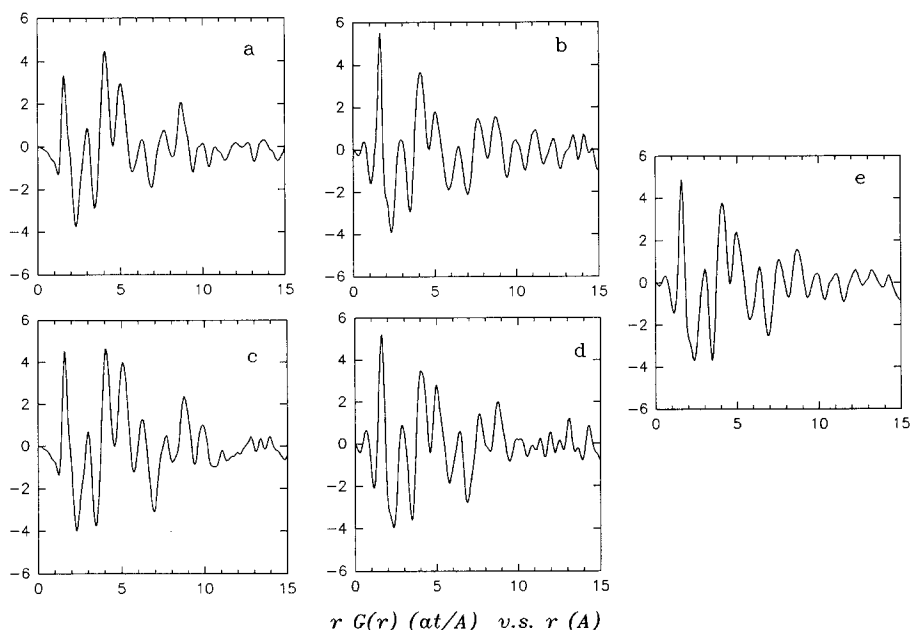
Fig. 3. $rG(r)$. (d) [S4], (b) [C4], (c) silica doped with a 10% molar of titania (sono-), (a) (classic), (e) vitreous silica. This function represents the difference between the RDF and an uniform distribution of local density, ρ_0, each peak corresponding to a coordination sphere. Those obtained for and silica gels doped with a 10 mol% of titania in similar experiments have been included for comparison. Beyond $r \sim 11$ Å, the short-range order is sharply lost in S samples and more gradually in C samples.

The RDF is calculated as

$$4\pi r^2\rho(r) = 4\pi r^2\rho_0 + rG(r),\qquad(1)$$

where ρ_0 and $\rho(r)$ represent, respectively, the mean and local atomic densities. $G(r)$ stands for the Fourier transform of the interference function,

$$G(r) = \int_0^{s_{max}}F(s)\ \sin(sr)\ ds.$$

To avoid the spurious oscillation due to the cut-off, data were extended up to $s_{max} = 40\ \text{Å}^{-1}$ by the method proposed by D'Anjou and Sanz [14].

The area beneath the first RDF (fig. 2) maximum is related to the average number of atoms in the first coordination sphere by [10]

$$A = \frac{1}{(\Sigma x_i Z_i)^2}\Sigma\Sigma x_i Z_i Z_j n_{ij}.\qquad(2)$$

Z_i is the i-element atomic number. n_{ij} are the averaged numbers of j-type atoms in the first coordination sphere of an i-type atom which are calculated from formulated hypothesis. The first

peak position indicates the most probable distance at which an atom can be found from an arbitrary atom taken as reference (table 1).

The reduced RDFs (fig. 3) show that a correspondence between gels and v-SiO_2 homologous peaks can be discerned up to r around 11–12 Å. Beyond this distance the short-range order is sharply lost in S samples and more gradually in the sample C.

4.2. NMR

The components (fig. 4) are easily identifiable as Q_2-type at about 89 ppm, Q_3-type at -100

Table 1
Structural parameters deduced from the RDF analysis

	Area (atom)	1st peak position (Å)	2nd peak position (Å)	Si–O–Si average bond angle ϕ (°)
Silica	2.99	1.61	3.10	148.6
C4	2.87	1.64	3.08	139.8
S4	2.97	1.64	3.10	141.9

Table 2
NMR analysis and specific surface areas

	δQ_2 (ppm)	δQ_3 (ppm)	δQ_4 (ppm)	$Q_2:Q_3:Q_4$	n_{OH}/n_{Si}	ϕ (°)	S (m²/g)
S2	−89.3	−100.1	−109.3	12:27:61	0.51	145.4	640
S6	−88.4	−99.2	−109.1	15:35:50	0.60	145.0	777
S10	−90.0	−99.8	−108.8	10:28:62	0.48	144.6	380
S14	−88.3	−99.5	−109.3	7:27:66	0.41	130.1	−
C2	−90.0	−99.7	−108.3	6:40:54	0.52	143.9	700
C6	−88.6	−100.1	−111.5	10:35:55	0.55	149.1	693

ppm and Q_4-type at −109 ppm (table 2), where the subscripts are the number of bridging oxygens surrounding the central silicon nucleus. For lack of a ^1H–^{29}Si double irradiation which corroborates it, it is supposed that there is $Si(OSi)_2(OH)_2$ or $Si(OSi)_3(OH)$ since they are located at −90.6 and −99.8 ppm. The more significant shift of the

peak maxima position can be observed in [C6], others are not representative.

4.3. Texture

Small angle X-ray scattering of sonogels show one crossover at about $q_1 = 0.07$ Å^{-1} [17], that correspond to correlation length of $r \sim 45$ Å.
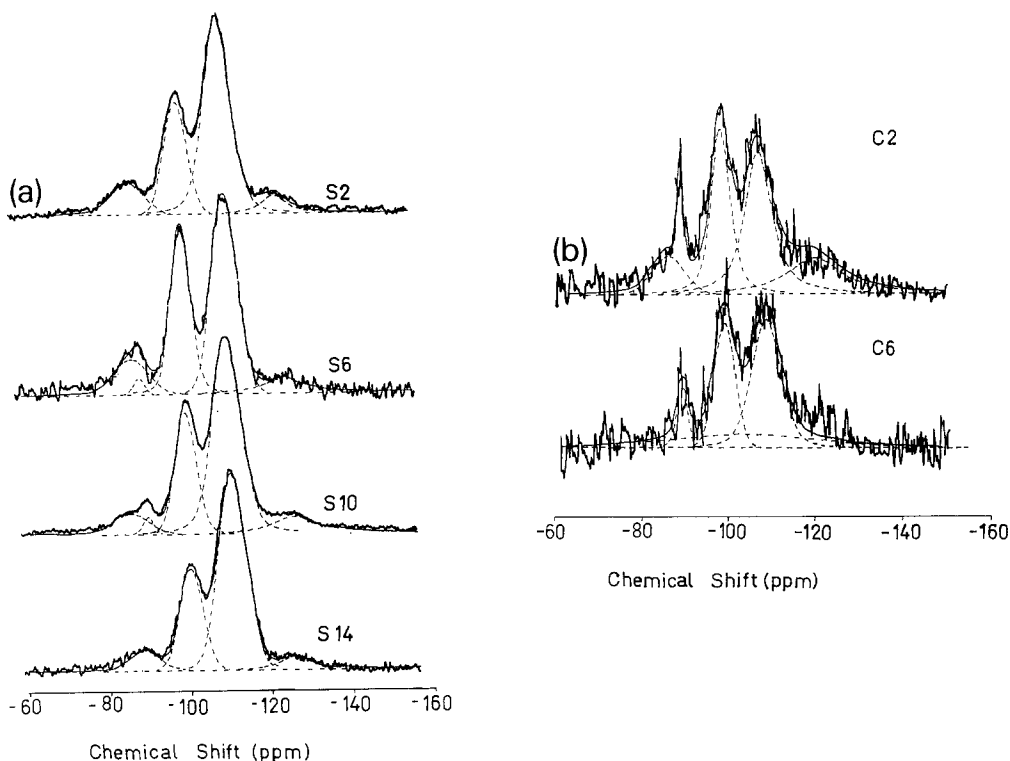
Fig. 4. MAS-NMR spectra of gels prepared with different amounts of hydrolysis water. (a) sono, (b) classics. Their more important characteristics are given in table 2. According to their estimated $Q_2:Q_3:Q_4$ ratios, ^{29}Si peak MAS show that the amount of hydrolysis water relatively affects the siloxane condensation and degree of crosslinking.

The specific surfaces measured by nitrogen fisisorption are shown in table 2.

On the basis of MEM, values of 63.0 ± 0.5 atom/nm^3 (2.09 g/$cm^3 \pm 0.02$) and 66.0 ± 0.5 atom/nm^3 (2.19 ± 0.02 g/cm^3) resulted for both [C4] and [S4] gels and silica glass microscopic density, respectively.

5. Discussion

The lower order of atomic arrangement inside the elementary particles with regard to v-SiO_2 is obvious from the scattered intensity maxima and the shift of these maxima toward high s values.

The behaviour of reduced RDF (fig. 3) can be interpreted as evidence of the different size distribution of the elementary particles which build up the gels: quite monodisperse in sonogel and polydisperse in their classical counterparts. At this point it is convenient to emphasize that data extension is only a tool to avoid meaningless oscillations to evaluate the main structural parameters. It does not affect the maximum correlation length up to which structural discussion is valid, which is determined by s_{min}, nor improve the resolution of the experiment.

A first approach to the gel atomic structure is to consider it as a silica network with a certain number of non-bridging oxygen (NBO). Under these conditions, if each atom has its bonds satisfied, except for an oxygen α fraction $0 < \alpha < 1$, the n_{ij} values are: $n_{11} = 0$, $n_{12} = 4$, $n_{21} = 2 - \alpha$, $n_{22} = 0$. The first maximum area may be expressed from eq. (2) as

$$A = 2.99 - 0.747\alpha.$$

According to the calculated values of A and the experimental error (± 0.1 atoms), this implies, taking into account the previously calculated skeletal densities, that n_{OH}/n_{Si} ([C4]) ~ 0.3 and n_{oH}/n_{Si} ([S4]) ~ 0.1. In the same way, from the specific surface areas (634 m^2/g for [S4] and 745 m^2/g for [C4]), the OH surface coverages, S_{OH}, (assuming that the whole of hydroxyls are on the gel surface) are $S_{OH} \sim 4$ and 2 OH/nm^2, respectively.

Hydroxyls induce elongations of adjacent Si–O bonds [15] that slightly affect the short-range

order and the backbone density. From the shape and size of the [S4] first RDF maximum, it can be stated that its short-range order, at the scale of first neighbours, is very close to v-SiO_2. At the second-neighbours level, a higher distortion of the tetrahedra arrangement caused by the finite size of the particles, in which the atoms are imbedded, is to be noted; the smaller the particles, the more important the disorder that this effect involves, as can be inferred from the flattening of the second RDF maximum, probably due to an overlapping of Si–O–Si and O–Si–O distances in tetrahedra with shared edges.

The Q_4 positions correspond to Si–O–Si average angle bonds ($\phi = -1.69$ (δ ppm)–39.3 [16] which abide by an imperceptible amount of three-membered rings on surface. The average number of silanol groups per Si atom, n_{OH}/n_{Si}, counting two per Q_2 site and one per Q_3 site, decreases when the sonogel was prepared with a water concentration much greater or much less than the stochiometric one. The samples prepared by the classic method had similar values.

The Q_4 and Q_3 peak heights are quite similar in [Cn] samples but in [Sn] samples Q_4 peak heights are much greater than Q_3's. However, the calculated OH concentrations per silicon atom are similar due to the relatively high value of Q_3. A calculation of the OH surface coverage can be made assuming a model of non-contacting spherical particles of 11 Å radius ($V/S = 0.365$ nm). For [S2] sample, it is calculated as

$$0.52 \frac{OH}{Si} \frac{6.02 \times 10^{23}}{60.084g} \frac{Si}{10^{21}} \frac{2.1g}{nm^3} \frac{V}{S} = 4.0 \frac{OH}{nm^2}.$$

In a similar way, for [S6], [S10] and [S14], values of 4.6, 3.7 and 3.1 OH/nm^2 result, respectively, which are not very far from the $\langle 111 \rangle$ face of β-cristobalite (4.55 OH/nm^2). If the BET measurements are taken into consideration, then the resulting values are 16.7 ([S2]), 12.9 ([S6]), 26.3 ([S10]), 7.8 ([C2]) and 8.0 ([C6]) (OH/nm^2), indicating an important number of silanols buried into the sonogel structure.

From WAXS and SAXS results, the sonogel structure can be described by a random close packing (RCP) of elementary particles of $r \approx 1.2$

nm forming clusters of $R \approx 4.5$ nm average radius. Since their packing fraction c (apparent-skeletal density ratio) is $0.38 < c < 0.47$ [2] and the maximum number of r radius spherical particles that can be packed in a spheroidal cluster of average radius $R = (4.5/1.2)r \approx 4r$ is $n = 0.74(R/r)^3 \approx 50$ with 12 contacts of each particle with other particles (N), in a RCP n, calculated as $(c/0.74) \times 50$, is $26 < n < 32$. The structure is not completely packed and there is an important number of mesopores. The small size of the particles also involves microporosity where hydroxyls may be trapped.

Considering the Avery–Ramsay relation [17], an aggregated coordination number of sonogels can be estimated as

$$N_n = \frac{4r_0}{0.375}\left(1 - \frac{S}{S_0}\right)$$

(where S_0 and r_0 are, respectively, the specific surface area and radius of an elementary particle) dividing the OH surface coverage ratios calculated from a model of non-contacting spheres and those evaluated from BET measurements. Then it results in $N_2 = 8.9$, $N_6 = 7.5$ and $N_{10} = 10.1$.

6. Conclusion

Both sonogels and classic gels are formed by elementary particles of 2.09 g/cm^3 density. The sonogel particles are monodisperse and smaller than those of the classic gel which explains the apparent high density and microporosity of those aerogels.

At a first-neighbour scale, the only noticeable changes in silica aerogels with respect to bulk vitreous silica come from the defects on the pore–matrix interface giving a longer average bond length and a decrease of the backbone density with regard to the bulk vitreous silica. At higher order neighbours, the finite size of the particle gives rise to a distortion in the tetrahedral vitreous silica network, more important in [Sn] samples.

The OH surface coverages are slightly higher in classic gel giving rise to a lower crosslinking. In sonogels, a considerable number of OH are buried in the microporous structure.

A sonogel can be described by a two level hierarchical model formed by clusters of 8 to 11 near-spherical particles of ~ 1.2 nm radius, homogeneously distributed.

References

[1] M. Tarasevich, Am. Ceram. Bull. 63 (1984) 500.
[2] Esquivias and J. Zarzycki, in: Ultrastructure Processing of Advanced Ceramics, ed. J.D. Mackenzie and D.R. Ulrich (Wiley, New York, 1987) p. 255.
[3] N. de la Rosa-Fox, L. Esquivias and J. Zarzycki, J. Mater. Sci. Lett. 10 (1991) 1237.
[4] J. Zarzycki, 5th Int. Conf. on Ultrastructure Processing of Ceramics, Glasses and Composites, Orlando, FL, Feb. 1991, in press.
[5] G.D. Scott, Nature 188 (1960) 908.
[6] N. de la Rosa-Fox, L. Esquivias and . Zarzycki, Diffusion Def. Data 53&54 (1987) 363.
[7] M. Piñero, M. Atik and J. Zarzycki, these Proceedings, p. 523.
[8] M. Atik and M. Aegerter, these Proceedings, p. 813.
[9] C. Bagnall and J. Zarzycki, SPIE (Sol–Gel Optics, San Diego CA, June (1990) 328 (1990) 108.
[10] B.E. Warren, X-Ray Diffraction (Addison-Wesley, New York, 1969).
[11] W. Wei, J. Non-Cryst. Solids 81 (1986) 239.
[12] J. More, B. Garbow and K. Hillstrom, User guide for Minckpack-1, National Laboratory Report ANL-80-74, Argonne, IL (1980).
[13] B. Himmel, Th. Gerber and H. Bürger, J. Non-Cryst. Solids 91 (1987) 122.
[14] A. D'Anjou and F. Sanz, J. Non-Cryst. Solids 28 (1978) 319.
[15] A.B. Rosenthal and S. Garofalini, J. Non-Cryst. Solids 107 (1988) 65.
[16] R. Oestrike, W.H. Yang, R.J. Kirkpatrick, R.L. Hervig, A. Navrotsky and B. Montez, Geochim. Cosmochim. Acta 51 (1987) 2199.
[17] R.G. Avery and J.D.F. Ramsay, J. Colloid. Interf. Sci. 42 (1973) 597.